

## Regulation of Alfvén Eigenmodes by Microturbulence in Fusion Plasmas

P. Liu<sup>1</sup>, X. Wei<sup>1</sup>, Z. Lin<sup>1,\*</sup>, G. Brochard<sup>1</sup>, G. J. Choi<sup>1</sup>, W. W. Heidbrink<sup>1</sup>, J. H. Nicolau<sup>1</sup>, and G. R. McKee<sup>2</sup>

<sup>1</sup>Department of Physics and Astronomy, University of California, Irvine, California 92697, USA

<sup>2</sup>College of Engineering, University of Wisconsin, Madison, Wisconsin 53706, USA



(Received 19 October 2021; revised 7 February 2022; accepted 6 April 2022; published 4 May 2022)

Global gyrokinetic simulations of mesoscale reversed shear Alfvén eigenmodes (RSAE) excited by energetic particles (EP) in fusion plasmas find that RSAE amplitude and EP transport are much higher than experimental levels at nonlinear saturation, but quickly diminish to very low levels after the saturation if background microturbulence is artificially suppressed. In contrast, in simulations coupling micro-meso scales, the RSAE amplitude and EP transport decrease drastically at the initial saturation but later increases to the experimental levels in the quasisteady state with bursty dynamics due to regulation by thermal ion temperature gradient (ITG) microturbulence. The quasisteady state EP transport is larger for a stronger microturbulence. The RSAE amplitude in the quasisteady state ITG-RSAE turbulence from gyrokinetic simulations, for the first time, agrees very well with experimental measurements.

DOI: 10.1103/PhysRevLett.128.185001

In magnetically confined fusion experiments, pressure gradients of energetic particles (EP) produced by fusion reactions or auxiliary heating can excite various Alfvén eigenmodes (AE) [1] with a characteristic size of energetic ion gyroradius (mesoscale), which can drive large EP transport that degrades plasma confinement and threaten machine integrity [2]. An outstanding issue of current interest is to identify important physical processes that determine nonlinearly saturated AE amplitude and associated EP transport level, which are needed for extrapolating EP confinement properties to burning plasma experiments such as ITER. Most first-principles simulations [3–8] of the AE saturation and EP transport have focused only on the AE nonlinear dynamics due to constraints of computing power and physics models.

Recent studies [9–13] have suggested possible effects of microturbulence [14] on the AE saturation and EP transport in fusion plasmas [9,11,13,15,16]. Pressure gradients of thermal particles excite various driftwave instabilities [14,17] with a characteristic size of thermal ion gyroradius (microscale), leading to ubiquitous microturbulence responsible for turbulent transport of thermal plasmas. The driftwave frequency is typically much smaller than the AE frequency. Despite the separation in the spatial and temporal scales, there can be strong cross-scale coupling between AE and microturbulence. Zonal flows can be nonlinearly generated by, and in turn, suppress both the AE [3,8,9,18,19] and microturbulence [20]. Microturbulence can damp the zonal flows and zonal structures [10] generated by the AE. EP scattering by the microturbulence [15,21] can affect phase space dynamics in nonlinear AE-EP interactions [11,13].

Understanding these cross-scale interactions requires global integrated simulations incorporating multiple

physical processes in a complex toroidal geometry and treating the dynamics of all particle species (EP, thermal ion, and electron) on an equal footing, a grand computational challenge. Validated multiscale simulations of fusion experiments that calculate unprecedented  $10^{16}$  particle-orbital steps have just become feasible on the world's fastest supercomputers using state-of-the-art global gyrokinetic toroidal code (GTC) [20] with comprehensive physics. In this work, GTC simulations find that microturbulence can play a critical role in regulating the AE turbulence, resulting in a larger EP transport for a stronger microturbulence even though the microturbulence directly drives little EP transport due to gyro-averaging effects as expected by the conventional wisdom [1,15]. This new paradigm opens research directions for studying cross-scale nonlinear interactions in fusion plasmas. The physics insights could also help understanding the cross-scale nonlinear interactions of energetic cosmic rays with Alfvén turbulence that are common in space and astrophysical plasmas [22].

*Global gyrokinetic simulations of RSAE.*—The equilibrium geometry and plasma profiles used in the simulations are taken from experimental equilibrium data of the DIII-D shot No. 159243 at 805 ms [23,24]. The RSAE is believed to degrade the EP confinement in this experiment [23]. The safety factor  $q$  has a reversed shear with a minimum value of  $q_{\min} = 2.94$  at  $\rho = 0.48$ , where  $\rho$  is the square root of toroidal flux normalized by its separatrix value. The radial simulation domain is  $\rho = [0.23, 0.78]$ . In GTC simulations with comprehensive physics [25], all species are described by the gyrokinetic model [26,27]. Beside perturbed electrostatic potential and parallel vector potential, compressible magnetic perturbation  $\delta B_{\parallel}$  [28] and equilibrium current [29] are incorporated in all simulations. The equilibrium

radial profiles of density and temperature for all species are fixed by a model particle and heat source. Based on convergence studies [24], GTC global field-aligned mesh consists of 32 parallel grids and  $2 \times 10^5$  perpendicular grids on the poloidal plane with a grid size  $\sim 0.6\rho_i$  to capture the short perpendicular wavelength of the ITG, where  $\rho_i \sim 2.1$  mm is the thermal ion gyroradius. Nonlinear electromagnetic simulations use 6000 particles per cell for each species with a local Maxwellian. The time step size is  $10^{-8}$  s to resolve the high frequency RSAE (60–110 kHz) and the electron thermal motion  $v_{th,e} \sim 2 \times 10^7$  m/s.

Using equilibrium geometry and kinetic EFIT [30] plasma profiles including fast ion density as shown in Figs. 2 and 3 of Ref. [24], earlier linear simulations [24,31] find that RSAE with low toroidal mode numbers are excited by the fast ions near the  $q_{min}$  flux surface with the most unstable toroidal mode number  $n = 4$ , an angular frequency  $\omega_4 = -4.28 \times 10^5$  rad/s, and a growth rate  $\gamma_4 = 3.4 \times 10^4$ /s. The thermal plasma pressure gradients drive the unstable ITG on both sides of the  $q_{min}$  surface with a growth rate  $\gamma_{16} = 2.5 \times 10^4$ /s and an angular frequency  $\omega_{16} = -8.16 \times 10^4$  rad/s for the toroidal mode number  $n = 16$ . The negative frequency indicates a wave propagating in the ion diamagnetic direction. These linear results have been verified in a careful benchmark [24] using eight simulation codes and validated by comparisons with experimental measurement [23] of the real frequency and mode structures from the electron cyclotron emission (ECE) [32] and electron cyclotron emission imaging (ECEI) measurement [33].

In the current study, the linearly most unstable  $n = 4$  RSAE is found to saturate by self-generated  $n = m = 0$  zonal flows and zonal structures [8]. Here,  $m$  is the poloidal harmonic. The RSAE saturates with a peak effective diffusivity of  $D_f = 15$  m<sup>2</sup>/s, which diminishes within about 0.1 ms due to coherent phase space structures formed by nonlinear wave-particle interactions [34]. Coulomb collisions have little effects in the simulation with the zonal flows, but have stronger effects in the simulation without the zonal flows, consistent with earlier simulations [5].

To study nonlinear RSAE couplings, we then simulate multiple toroidal modes of  $n = [0, 10]$ . As shown in Fig. 1(a), the electrostatic potentials  $\delta\phi$  (normalized by electron temperature  $T_e$  and charge  $e$ ) of dominant  $n = 4$  and 5 modes at the  $q_{min}$  surface grow to large amplitudes and saturate by the self-generated zonal flows and zonal structures. Less unstable modes such as  $n = 3$  and stable modes such as  $n = 2$  are generated by nonlinear coupling of the dominant modes. The RSAE saturates at a lower amplitude with a peak effective EP diffusivity of  $D_f = 8$  m<sup>2</sup>/s as shown in Fig. 1(b). However, both RSAE amplitude and EP diffusivity at the saturation are much higher than the experimental levels [35]. After the

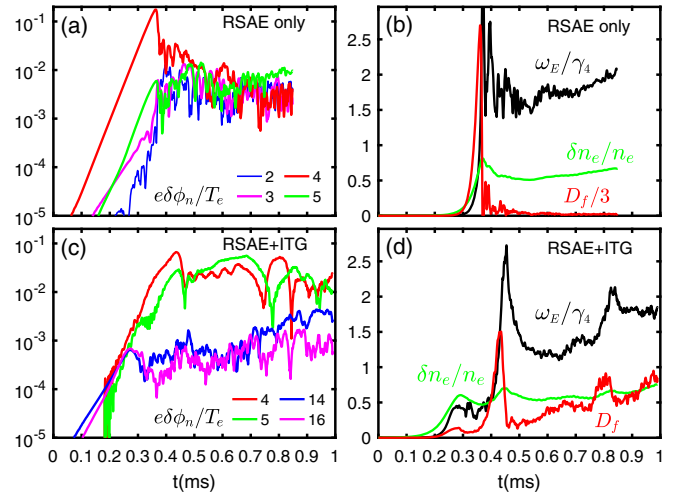


FIG. 1. Time history of perturbed electrostatic potentials  $e\delta\phi/T_e$  for RSAE ( $n = 2 - 5$ ) from simulation of RSAE only [panel (a)] and for ITG ( $n = 14, 16$ ) from simulation of ITG-RSAE [panel (c)]. Corresponding zonal flow shearing rate  $\omega_E/\gamma_4$ , electron density perturbation  $\delta n_e/n_e$  (%), and effective EP diffusivity  $D_f$  (m<sup>2</sup>/s) are shown in panel (b) and panel (d).

nonlinear saturation, the effective diffusivity diminishes within about 0.05 ms even with high levels of the density fluctuation  $\delta n_e$  and the zonal potential  $\phi_{00}$ , represented by shearing rate  $\omega_E = -R^2 B_\theta (\partial^2 \phi_{00} / \partial \psi^2)$ . This indicates that coherent structures in the EP phase space persist because of the dominance of the  $n = 4$  mode, which flattens gradients of the EP distribution function at the resonances even in the presence of multiple toroidal modes. Here,  $D_f$ ,  $\omega_E$ , and  $\delta n_e$  are root-mean-square (rms) values averaged over the radius domain of the major radius  $R = [195, 204]$  cm. This nonlinear dynamic of a huge initial burst followed by a quickly diminished AE amplitude and EP transport has also been observed in other global simulations [3,7,8,12,18]. Therefore, nonlinear coupling of multiple toroidal modes and zonal flow effects cannot explain the RSAE amplitude and EP transport measured in the DIII-D experiments.

*Multiscale simulations coupling ITG-RSAE.*—We now study effects of background ITG turbulence on the RSAE turbulence. Microturbulence is ubiquitous in the tokamak and often manifests itself as electron density fluctuations over the whole plasma volume throughout the entire discharge. On the other hand, RSAE typically appears intermittently in time and localizes near the  $q_{min}$  surface. To provide a background ITG turbulence, we initiate an electromagnetic simulation of the ITG turbulence by using Fourier filtering to remove all fluctuating fields of the  $n = [1, 10]$  RSAE and keep only the  $n = [11, 25]$  ITG and the  $n = 0$  zonal mode. The ITG instability grows on both sides of the  $q_{min}$  surface [31] and saturates by the self-generated zonal flows [20]. Then the ITG turbulence spreads [36] across the whole radial domain, resulting in a radially

uniform turbulence intensity in the steady state. Figure 1(c) shows that the most unstable ITG modes ( $n = 14, 16$ ) saturate at  $t \approx 0.28$  ms, which induces a large electron density fluctuation of  $\delta n_e/n_e \sim 0.6\%$  but a small EP diffusivity as shown in Fig. 1(d). The ITG-driven EP diffusivity of  $D_f \approx 0.11$  m<sup>2</sup>/s at time  $t \approx 0.28$  ms is consistent with earlier GTC simulations [21] and experimental modeling [15].

We add the RSAE shortly before the ITG saturation by allowing the  $n = [1, 10]$  modes in the self-consistent simulation. The background ITG turbulence slightly reduces (by 10%) the growth rates of the most unstable RSAE modes ( $n = 4, 5$ ) in the linear phase. The RSAE saturates at  $t \approx 0.43$  ms with an amplitude of the electrostatic potential much larger than the ITG turbulence [Fig. 1(c)], but with an amplitude of the electron density perturbation smaller than the ITG turbulence [Fig. 1(d)]. At the RSAE saturation ( $t \approx 0.43$  ms), the effective EP diffusivity increases to  $D_f \approx 1.5$  m<sup>2</sup>/s, which is much smaller (by a factor of 5) than that in the simulation of the RSAE turbulence only [Fig. 1(b)]. The saturation amplitude of the dominant  $n = 4$  RSAE also decreases by a factor of more than 2. Both simulations have similar zonal flow shearing rates at the RSAE saturation, which are much larger than that generated by the ITG turbulence. Therefore, the background ITG turbulence significantly reduces the initial saturation amplitude, most likely through EP scattering by the ITG turbulence that breaks the EP-RSAE resonance.

The most striking effects of the background ITG turbulence are that the RSAE turbulence can maintain a quasisteady state with the RSAE amplitude and EP diffusivity consistent with experiments. In contrast to the quickly diminished EP diffusivity in the simulation of the RSAE turbulence only [Fig. 1(b)], EP diffusivity maintains a quasisteady state in the coupled ITG-RSAE simulation as shown in Fig. 1(d). There are nonlinear oscillations in the zonal flow amplitude, EP diffusivity, and RSAE mode amplitudes, which suggest that EP scattering by the ITG turbulence may destroy coherent structures in the EP phase space and damp the zonal flows.

In the quasisteady state, the mesoscale RSAE and microscale ITG turbulence coexist and nonlinearly interact with each other as illustrated by the poloidal contour plots of the perturbed electrostatic potential and electron density in Fig. 2. The electrostatic potential  $\delta\phi$  is dominated by the low- $n$  RSAE, which peaks at the  $q_{\min}$  surface with a weak ballooning structure. On the other hand, the electron density perturbation  $\delta n_e$  is dominated by the high- $n$  ITG modes with a strong ballooning structure, which is asymmetrical about the  $q_{\min}$  flux surface due to the positive and negative magnetic shear on each side. The simulation results that the low- $n$  RSAE turbulence dominates the electrostatic potential but the high- $n$  ITG turbulence dominates the electron density perturbation are consistent with the fact that the ITG instability is mostly electrostatic but

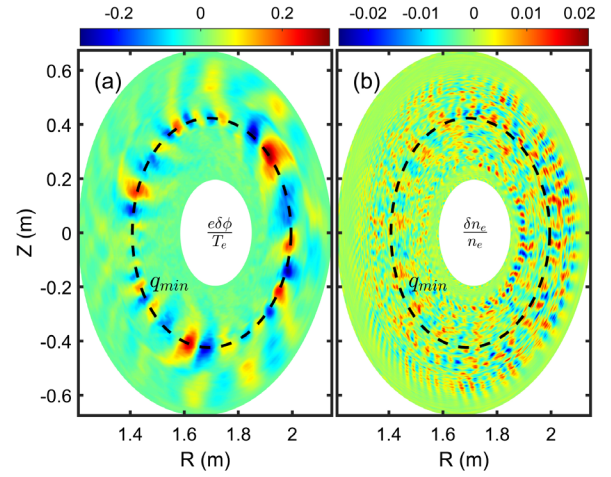


FIG. 2. Poloidal contour plots of perturbed electrostatic potential  $e\delta\phi/T_e$  [panel (a)] and electron density perturbation  $\delta n_e/n_e$  [panel (b)] at  $t = 0.78$  ms from simulation coupling ITG-RSAE turbulence.

the RSAE has a polarization close to the shear Alfvén wave, which is nearly incompressible [1].

*Comparisons with experiments.*—The results from the GTC simulation coupling ITG-RSAE turbulence compare very well with the DIII-D experimental measurements [23]. Figure 3(a) shows the simulated density fluctuation  $\delta n_e$  spectra in two regions of  $R = [198, 205]$  and  $R = [205, 212]$  cm, which are consistent with the experimental observation of  $k_{\theta}\rho_i < 0.5$  by the 64-channel beam emission spectroscopy (BES) measurements. The inner region covers the  $q_{\min}$  surface, where the spectrum has two peaks with the long wavelength modes  $k_{\theta}\rho_i = 0.11$  corresponding to the RSAE and the short wavelength modes  $k_{\theta}\rho_i = 0.38$  corresponding to the inner ITG. In the outer region, the RSAE amplitude is very small and the density spectrum peaks only at the short wavelength modes  $k_{\theta}\rho_i = 0.41$  corresponding to the outer ITG.

The most remarkable agreement between the simulation and experiment is the RSAE amplitude and mode structure. In Fig. 3(b), the radial profiles of the  $n = 4$  mode (including

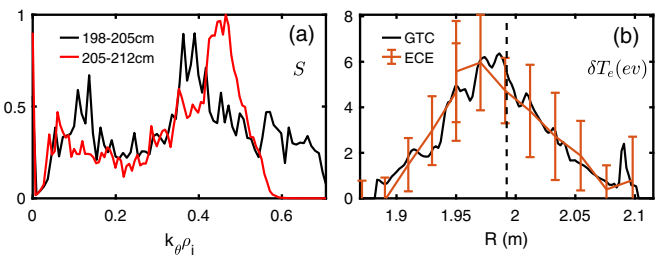


FIG. 3. Spectrum  $S$  of electron density perturbation  $\delta n_e$  as a function of poloidal wave number  $k_{\theta}\rho_i$  in two radial regions [panel (a)], and radial profiles of electron temperature perturbation  $\delta T_e$  [panel (b)] from GTC simulations and ECE measurements in DIII-D.

all  $m$  harmonics) of the electron temperature perturbation  $\delta T_e$  from the simulation shows, for the first time, excellent agreement with the ECE measurement. Here, the radial profiles of  $\delta T_e$  is averaged over  $t = [0.7, 0.8]$  ms in the simulation. The corresponding magnetic perturbation is  $\delta B/B_0 \sim 1.1 \times 10^{-3}$ . While a longer simulation duration is required for the steady-state transport, the estimated effective EP diffusivity of  $D_f \approx 0.8 \text{ m}^2/\text{s}$  has the right order of magnitude to the fast ion transport inferred from measured neutrons but is below the interpretive modeling value of  $2.5 \text{ m}^2/\text{s}$  [35]. The interpretive modeling shows that additional EP transport is driven by toroidal Alfvén eigenmodes (TAE) [24,35] in the outer region due to steepened fast ion pressure profile, which is not taken into account in the GTC simulations. Finally, simulations use an isotropic EP distribution, which may cause some differences in the RSAE amplitude and EP transport since the injected neutral beam population is not isotropic.

*Dependence of RSAE turbulence on ITG turbulence intensity.*—Considering uncertainties in the experimental measurements of plasma profiles, we perform simulations with a weaker or stronger thermal ion temperature gradient  $\nabla T_i$  but keeping all other plasma profiles unchanged. In Figs. 4(a) and 4(b), simulation using a weaker gradient ( $0.8\nabla T_i$ ) shows a smaller ITG growth rate of  $1.9 \times 10^4/\text{s}$  and density perturbation amplitude of 0.5% in the quasisteady state. The linear RSAE growth rate decreases less than 5%. However, the nonlinear RSAE turbulence and EP transport change more significantly compared with the simulation using the experimental value of the  $\nabla T_i$ . In particular, effective EP diffusivity increases by 70% at the

RSAE saturation but decreases by more than a factor of 2 in the quasisteady state. Therefore, the nonlinear effects of this slightly weaker background ITG turbulence on the RSAE turbulence are much weaker. Consistently, in the simulation using a stronger gradient ( $1.3\nabla T_i$ ) shown in Figs. 4(c) and 4(d), the slightly stronger background ITG turbulence has much stronger nonlinear effects on the RSAE turbulence. With this stronger gradient of  $1.3\nabla T_i$ , the ITG growth rate increases to  $4.0 \times 10^4/\text{s}$  and the density perturbation amplitude to 0.8%. The linear RSAE growth rate increases less than 5%. However, the EP diffusivity decreases significantly at the initial RSAE saturation but exhibits another burst, resulting in an overall higher transport in the quasisteady state. Note that the initial saturation level is physically meaningful because of the bursty dynamics. The density fluctuation amplitude of 0.5%–0.8% from gyrokinetic simulations is within a reasonable range of the BES integrated low- $k$  density fluctuation amplitude measurement of 0.3%–0.4%.

Furthermore, the second burst of the RSAE amplitude and EP diffusivity occurs when the zonal flows generated by the RSAE decrease to a lower level in the presence of the background ITG turbulence, which leads to an intermittency in the EP transport. Figures 1 and 4 show that the RSAE nonlinearly saturates when the instantaneous zonal flow shearing rate rises to a high level of  $\omega_E = 2.5\gamma_4$  and that the unstable RSAE grows exponentially again when the shearing rate is damped by the background ITG turbulence to a low level of  $\omega_E = \gamma_4$ . When the ITG turbulence intensity is higher, the damping of the zonal flows is stronger and the oscillation period is shorter for the zonal flows, RSAE amplitude, and EP diffusivity. Since zonal flows are mostly generated by the RSAE turbulence, this regulation could arise from the radial scattering of the EP and thermal plasmas by the background ITG turbulence, which induces the radial diffusion of the zonal density. These simulation results are consistent with experimental observations of the intermittency in the RSAE amplitudes due to the lower microturbulence intensity in the DIII-D experiments with negative triangularity [11,16]. The GTC simulation results finding strong coupling between AE and microturbulence are also consistent with simulations by other gyrokinetic continuum [9] and particle [12] codes.

The conjecture that the scattering of the EP and thermal plasmas by the background ITG turbulence dominates the regulation of the RSAE turbulence is further supported by the relevant time scales calculated from the coupled ITG-RSAE simulation. The dominant EP-RSAE resonance in this experiment is toroidal precessional resonance [31] with the action-angle variables of  $(P_\zeta, \zeta)$ , where  $\zeta$  is the toroidal angle. The canonical angular momentum  $P_\zeta$  is dominated by the poloidal flux function, which can undergo a random walk due to the EP radial diffusion by the ITG turbulence [21]. This EP scattering rate by the ITG turbulence is  $\omega_{fs} = k_\perp^2 D_f \sim 280/\text{s}$  for the EP with a kinetic energy of 20 keV,

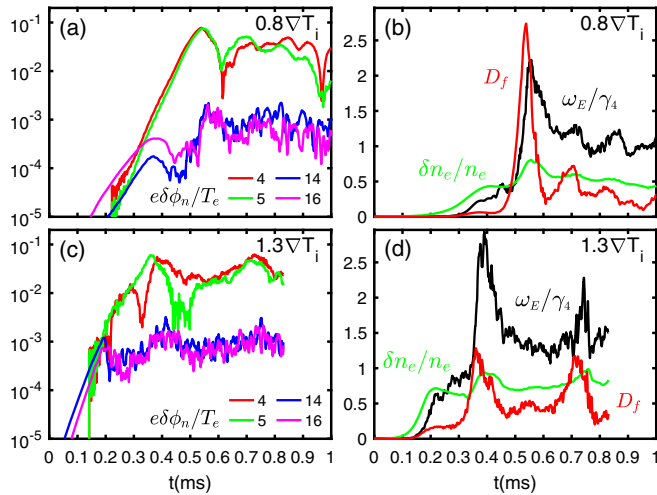


FIG. 4. Time history of perturbed electrostatic potentials  $e\delta\phi/T_e$  for RSAE ( $n = 4, 5$ ), and ITG ( $n = 14, 16$ ) from simulations with a weaker [panel (a) using  $0.8\nabla T_i$ ] or stronger [panel (c) using  $1.3\nabla T_i$ ] thermal ion temperature gradient. Corresponding zonal flow shearing rate  $\omega_E/\gamma_4$ , electron density perturbation  $\delta n_e/n_e$  (%), and effective EP diffusivity  $D_f$  ( $\text{m}^2/\text{s}$ ) are shown in panels (b) and (d).

which is much larger than the Coulomb collision frequency of  $\nu_f \sim 20/s$  for the same kinetic energy. Since resonant EPs only occupy a small region of the EP phase space, the effective ITG scattering rate and Coulomb collision frequency can be much larger. If we use a heuristic factor of  $(\omega_4/\gamma_4)^2$  to estimate this amplifying effect, the effective ITG scattering rate is  $(\omega_4/\gamma_4)^2\omega_{fs} \sim 1.3\gamma_4$  and the effective Coulomb collision frequency is  $(\omega_4/\gamma_4)^2\nu_f \sim 0.09\gamma_4$ . Therefore, effects of the Coulomb collisions are negligible, which is consistent with the simulations finding no effects of Coulomb collisions when using the realistic collision frequency. On the other hand, effects of EP scattering by the ITG turbulence are much stronger since the effective scattering rate is close to the RSAE growth rate and the zonal flow shearing rate.

The authors thank M. E. Austin for the ECE data. This work was supported by DOE SciDAC ISEP and INCITE, and used computing resources at ORNL (DOE Contract DE-AC05-00OR22725) and NERSC (DOE Contract DE-AC02-05CH11231), and experimental data from DIII-D National Fusion Facility (DOE Contract DE-FC02-04ER54698).

---

\*zhihongl@uci.edu

- [1] L. Chen and F. Zonca, *Rev. Mod. Phys.* **88**, 015008 (2016).
- [2] A. Fasoli *et al.*, *Nucl. Fusion* **47**, S264 (2007).
- [3] D. A. Spong, B. A. Carreras, and C. L. Hedrick, *Phys. Plasmas* **1**, 1503 (1994).
- [4] S. D. Pinches, L. C. Appel, J. Candy, S. E. Sharapov, H. L. Berk, D. Borba, B. N. Breizman, T. C. Hender, K. I. Hopcraft, G. T. A. Huysmans, and W. Kerner, *Comput. Phys. Commun.* **111**, 133 (1998).
- [5] J. Lang, G.-Y. Fu, and Y. Chen, *Phys. Plasmas* **17**, 042309 (2010).
- [6] H. S. Zhang, Z. Lin, and I. Holod, *Phys. Rev. Lett.* **109**, 025001 (2012).
- [7] G. Vlad, S. Briguglio, G. Fogaccia, V. Fusco, C. Di Troia, E. Giovannozzi, X. Wang, and F. Zonca, *Nucl. Fusion* **58**, 082020 (2018).
- [8] Y. Chen, G. Y. Fu, C. Collins, S. Taimourzadeh, and S. E. Parker, *Phys. Plasmas* **25**, 032304 (2018).
- [9] E. M. Bass and R. E. Waltz, *Phys. Plasmas* **17**, 112319 (2010).
- [10] F. Zonca, L. Chen, S. Briguglio, G. Fogaccia, G. Vlad, and X. Wang, *New J. Phys.* **17**, 013052 (2015).
- [11] V. N. Duarte, H. L. Berk, N. N. Gorelenkov, W. W. Heidbrink, G. J. Kramer, R. Nazikian, D. C. Pace, M. Podestà, B. J. Tobias, and M. A. Van Zeeland, *Nucl. Fusion* **57**, 054001 (2017).
- [12] A. Biancalani *et al.*, *Plasma Phys. Controlled Fusion* **63**, 065009 (2021).
- [13] N. N. Gorelenkov and V. N. Duarte, *Phys. Lett. A* **386**, 126944 (2021).
- [14] W. Horton, *Rev. Mod. Phys.* **71**, 735 (1999).
- [15] W. W. Heidbrink, J. M. Park, M. Murakami, C. C. Petty, C. Holcomb, and M. A. Van Zeeland, *Phys. Rev. Lett.* **103**, 175001 (2009).
- [16] M. A. Van Zeeland *et al.*, *Nucl. Fusion* **59**, 086028 (2019).
- [17] W. M. Tang, *Nucl. Fusion* **18**, 1089 (1978).
- [18] Y. Todo, H. L. Berk, and B. N. Breizman, *Nucl. Fusion* **50**, 084016 (2010).
- [19] H. Zhang and Z. Lin, *Plasma Sci. Technol.* **15**, 969 (2013).
- [20] Z. Lin *et al.*, *Science* **281**, 3 (1998).
- [21] W. Zhang, Z. Lin, and L. Chen, *Phys. Rev. Lett.* **101**, 095001 (2008).
- [22] J. Giacalone and J. R. Jokipii, *Astrophys. J.* **520**, 204 (1999).
- [23] C. S. Collins, W. W. Heidbrink, M. E. Austin, G. J. Kramer, D. C. Pace, C. C. Petty, L. Stagner, M. A. Van Zeeland, R. B. White, and Y. B. Zhu, *Phys. Rev. Lett.* **116**, 095001 (2016).
- [24] S. Taimourzadeh *et al.*, *Nucl. Fusion* **59**, 066006 (2019).
- [25] I. Holod, W. L. Zhang, Y. Xiao, and Z. Lin, *Phys. Plasmas* **16**, 122307 (2009).
- [26] W. W. Lee, *Phys. Fluids* **26**, 556 (1983).
- [27] A. J. Brizard and T. S. Hahm, *Rev. Mod. Phys.* **79**, 421 (2007).
- [28] G. Dong, J. Bao, A. Bhattacharjee, A. Brizard, Z. Lin, and P. Porazik, *Phys. Plasmas* **24**, 081205 (2017).
- [29] W. Deng, Z. Lin, and I. Holod, *Nucl. Fusion* **52**, 023005 (2012).
- [30] L. L. Lao, H. St. John, R. D. Stambaugh, A. G. Kellman, and W. Pfeiffer, *Nucl. Fusion* **25**, 1611 (1985).
- [31] H. Wang, P. Liu, Z. Lin, and W. Zhang, *Plasma Sci. Technol.* **23**, 015101 (2021).
- [32] M. E. Austin and J. Lohr, *Rev. Sci. Instrum.* **74**, 1457 (2003).
- [33] B. Tobias *et al.*, *Rev. Sci. Instrum.* **81**, 10D928 (2010).
- [34] H. L. Berk and B. N. Breizman, *Phys. Fluids B* **2**, 2246 (1990).
- [35] W. W. Heidbrink, C. S. Collins, M. Podestà, G. J. Kramer, D. C. Pace, C. C. Petty, L. Stagner, M. A. Van Zeeland, R. B. White, and Y. B. Zhu, *Phys. Plasmas* **24**, 056109 (2017).
- [36] Z. Lin, S. Ethier, T. S. Hahm, and W. M. Tang, *Phys. Rev. Lett.* **88**, 195004 (2002).